UDC 544.228

DOI: 10.15372/CSD2019141

Morphological Design of Nanocrystalline Cerium Dioxide during Thermal Decomposition of Cerium (III) Oxalate Decahydrate

D. V. MASLENNIKOV[1,2], A. A. MATVIENKO[1,2], A. A. SIDELNIKOV[1,2], S. A. CHIZHIK[1,2]

[1]*Institute of Solid State Chemistry and Mechanochemistry, Siberian Branch of the Russian Academy of Sciences, Novosibirsk, Russia*

E-mail: daniel@solid.nsc.ru

[2]*Novosibirsk State University, Novosibirsk, Russia*

Abstract

Materials based on cerium dioxide are used in various fields of high-tech industry: from precision polishing of optical glasses and the production of high-strength ceramics to using them as three-route catalysts in engines and medical applications as biomimetics. Due to a wide range of practical applications of such materials, there is an actual task to develop a method for producing cerium oxide with the ability to control its textural characteristics. To solve this problem in this work, the method of thermal decomposition of the precursor $Ce_2(C_2O_4)_3 \cdot 10H_2O$ was chosen. The main advantage of this method is the possibility of obtaining products in the form of a pseudomorph consisting of nanoparticles of the product and preserving the shape and size of the crystals. In the course of the work, the conditions for obtaining pseudomorph were found, i.e. porous granules of cerium oxide nanoparticles, the size of which is set at the stage of synthesis of precursor crystals. Techniques have been developed for growing $Ce_2(C_2O_4)_3 \cdot 10H_2O$ crystals of various sizes and habit. The work also revealed the factors that influence the textural characteristics of the resulting oxides during thermal decomposition of the selected precursor. It was shown that during thermal decomposition of thin (<20 μm) precursor plates with a basal face (010) in air, cerium dioxide pseudomorph transparent to visible light was formed. Thicker crystals were destroyed parallel to the (010) face with a fracture scale of about 10 μm. It was shown that an increase in water vapor pressure during dehydration led to structural changes other than those during dehydration in air. With such a rearrangement of the structure, the initial crystals are destroyed into particles less than 5 μm. In this work, we were able to obtain a pseudomorph consisting of 5–6 nm particles of cerium dioxide with a surface area of 140–150 m^2/g and 40 % porosity. Controlled annealing allowed the microstructure to be enlarged to the required size of crystallites that make up the pseudomorph.

Keywords: cerium oxalate, nanocrystalline cerium oxide, pseudomorph, thermal decomposition

INTRODUCTION

At present, cerium dioxide CeO_2 is widely used in various areas of science and industry. A unique property of this compound is its ability to easily change the degree of cerium oxidation from +4 to +3 and back, which allows this compound to catalyze both oxidation and reduction processes. This feature is used, for example, in automobile engines. Materials based on cerium dioxide act as three-route catalysts accelerating at the same time the reduction of nitrogen oxide (II) into nitrogen, oxidation of carbon monoxide into carbon dioxide, and after-burning of gaseous hydrocarbons [1]. In addition, CeO_2 is used as a catalyst and catalyst support in the reactions of selective oxidation and dehydrogenation [2, 3]. Cerium dioxide doped with the metals with the oxidation degree lower than +4 (for example, Sm^{3+}, Gd^{3+}) is a good oxygen conductor used as

the electrolyte in solid oxide fuel elements [4, 5]. Cerium dioxide is also widely used as an abrasive-polishing material [6], in electrochromic coatings and sensors [7], in protective coatings absorbing UV radiation [8, 9]. During recent years, a large number of works dealing with the studies of the antioxidant properties of this compound have been published. It was demonstrated that the nanoparticles of cerium dioxide are able to bind various types of free radicals in an organism [10, 11]. So, nanosized CeO_2 may become promising medicine against the diseases caused by oxidative stress, including the diseases of skin, heart, Alzheimer disease and even obesity [12, 13].

Definite texture characteristics of this material are necessary in different areas of cerium dioxide application. For example, CeO_2 with high porosity and specific surface is required for catalysis, separate nanoparticles able to penetrate through the phospholipid membranes of cells are necessary in medicine, while the particles of micrometer size are necessary in the case if cerium dioxide is used as an efficient polishing material.

Various methods of obtaining CeO_2 nanoparticles are known. Among them, the methods of synthesis in aqueous and anhydrous media are most widespread: first of all, the direct precipitation of hydrated cerium dioxide from the solutions of cerium salts with the addition of strong bases [14], homogeneous hydrolysis [15], synthesis in microemulsions and reverse micelles [16, 17] *etc.*

In the present work, to obtain nanosized cerium dioxide, we chose the thermal decomposition of precursor, which is cerium (III) oxalate decahydrate $Ce_2(C_2O_4)_3 \cdot 10H_2O$. Thermal decomposition of solids is one of the traditional methods of solid state chemistry for the synthesis of the particles of small size. This is a simple and available method allowing one to obtain nanoparticles of various substances [18]. As a rule, the product of thermal decomposition is a porous compact formation retaining the shape of the initial particle of the precursor. This macrostructure of the product is called pseudomorph in topochemical literature. In the pseudomorph, the nanoparticles of the product are bound with each other through strong contacts and form a porous three-dimensional framework, 3D-nanostructure. As a rule, the volume of voids (pores) is comparable with (or even exceeds) the volume of the solid substance. So, the final product is a porous agglomerate of nanoparticles, which may be interesting in various applications, for example in catalysis. Previously, the authors of the present paper proposed an approach described in [19, 20], allowing prediction of pseudomorph parameters. According to this approach, the total pore volume in a pseudomorph is determined by the volume shrinkage during the reaction, pore size distribution is determined by the stage sequence of the reaction and shrinkage at every stage of the reaction, and the size of product particles is determined by the largest shrinkage among those for different stages of the reaction.

In the present work, we generalize our previous experimental results on the studies of thermal decomposition of cerium oxalate decahydrate [19, 21, 22]. The major attention was paid to the analysis of determining morphological changes during the reaction. The possibilities of morphological design of the final product, CeO_2 pseudomorph, are presented, under the change of conditions at each of the following stages: the growth of precursor crystals, dehydration of the resulting crystals, oxidative thermolysis of dehydrated oxalate, and annealing of the resulting cerium dioxide.

EXPERIMENTAL

The morphology of initial crystals and reaction products was studied with the help of optical polarization-interference microscopes Biolar (PZO, Poland), Polam L-213 (LOMO, the USSR), reflected-light optical microscope Neophot 21 (Carl-Zeiss, Germany), scanning electron microscope TM-1000 (Hitachi, Japan). High-resolution electron microphotographs and micro-diffraction patterns of the products of oxidative thermolysis were taken with the help of a transmission electron microscope JEM-2200 FS (Jeol, Japan).

To obtain the information about the changes in morphology during thermal decomposition of the precursor, *in situ* optical investigation of precursor crystals during heating was carried out. The details of the experiment were presented in [22].

Thermogravimetric measurements were carried out with the help of thermobalance SETARAM B70 (France) in air. Simultaneous TG-DSC analysis with mass spectrometry was carried out with a STA-449F1 instrument (Netzsch, Germany) with heating rates 3–5 °C/min in a mixture of argon with oxygen (80 % Ar + 20 % O_2). The results of thermal analysis were presented in [21, 22].

The data on the specific surface of the samples and the isotherms of nitrogen adsorption-desorption were obtained with a TermoSorb instrument (Russia) and an automated adsorption set-up ASAP 2400 (the USA).

Powder diffraction patterns were obtained using a D8 Advance diffractometer (Bruker, Germany). *In situ* diffraction studies during heating in the air and in vacuum were carried out in a high-temperature chamber HTK 1200 N (Anton Paar, Austria, temperature stability ±0.1 °C; the cell was made of Al_2O_3).

The procedures of crystal growth and the conditions of thermal decomposition were described in [21, 22].

RESULTS AND DISCUSSION

Oxalates of lanthanoids from La to Er form isostructural decahydrates [23]. The data on the structure of cerium (III) oxalate decahydrate were presented in [24]. The structure belongs to the monoclinic system and has a space group of symmetry $P2_1/c$. Each Ce^{3+} cation is surrounded by three oxalate groups and three water molecules (Fig. 1, *a*). So, the coordination number of cerium is equal to 9. Oxalate ion in this structure is a bidentate ligand, so each oxalate anion coordinates two cerium cations. This is how the hexagonal cerium oxalate layer, a basic structural element, is formed (see Fig. 1, *c*). The layers are perpendicular to the *b* axis and are superimposed on each other with a shift along the *c* axis. The rest water molecules (for decahydrate, there are two such molecules per each cerium cation) are arranged inside the layers and between them. Thermal decomposition of $Ce_2(C_2O_4)_3 \cdot 10H_2O$ during heating in the air proceeds in two main stages: dehydration and oxidative thermolysis of oxalate. Dehydration is a multistage process that includes the formation of several intermediate hydrates. The final product of the reaction is CeO_2. The total volume change during the reaction is about 85 %.

Dehydration in vacuum or in the air involves uniform compression of thin crystals without destruction (Fig. 2, *c*, *d*) or cracking into large blocks (larger than 10 μm) thick crystals with the formation of the pseudomorph (see Fig. 2, *b*). During

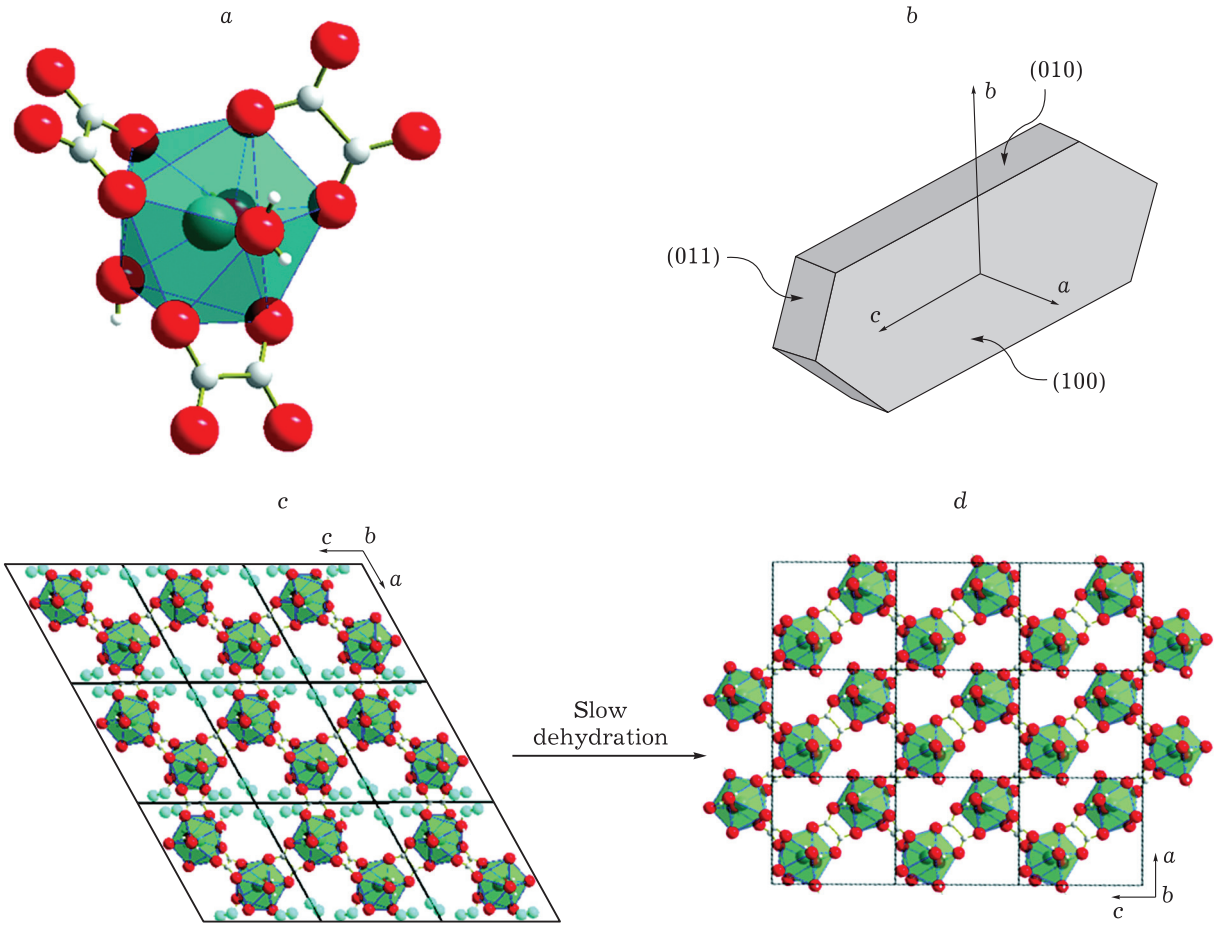

Fig. 1. Structural data for initial $Ce_2(C_2O_4)_3 \cdot 10H_2O$ (*a* – structure of the coordination polyhedron around Ce^{3+}, *b* – crystal facing, *c* – structure of the layer) and intermediate product $Ce_2(C_2O_4)_3 \cdot 6H_2O$ (*d*).

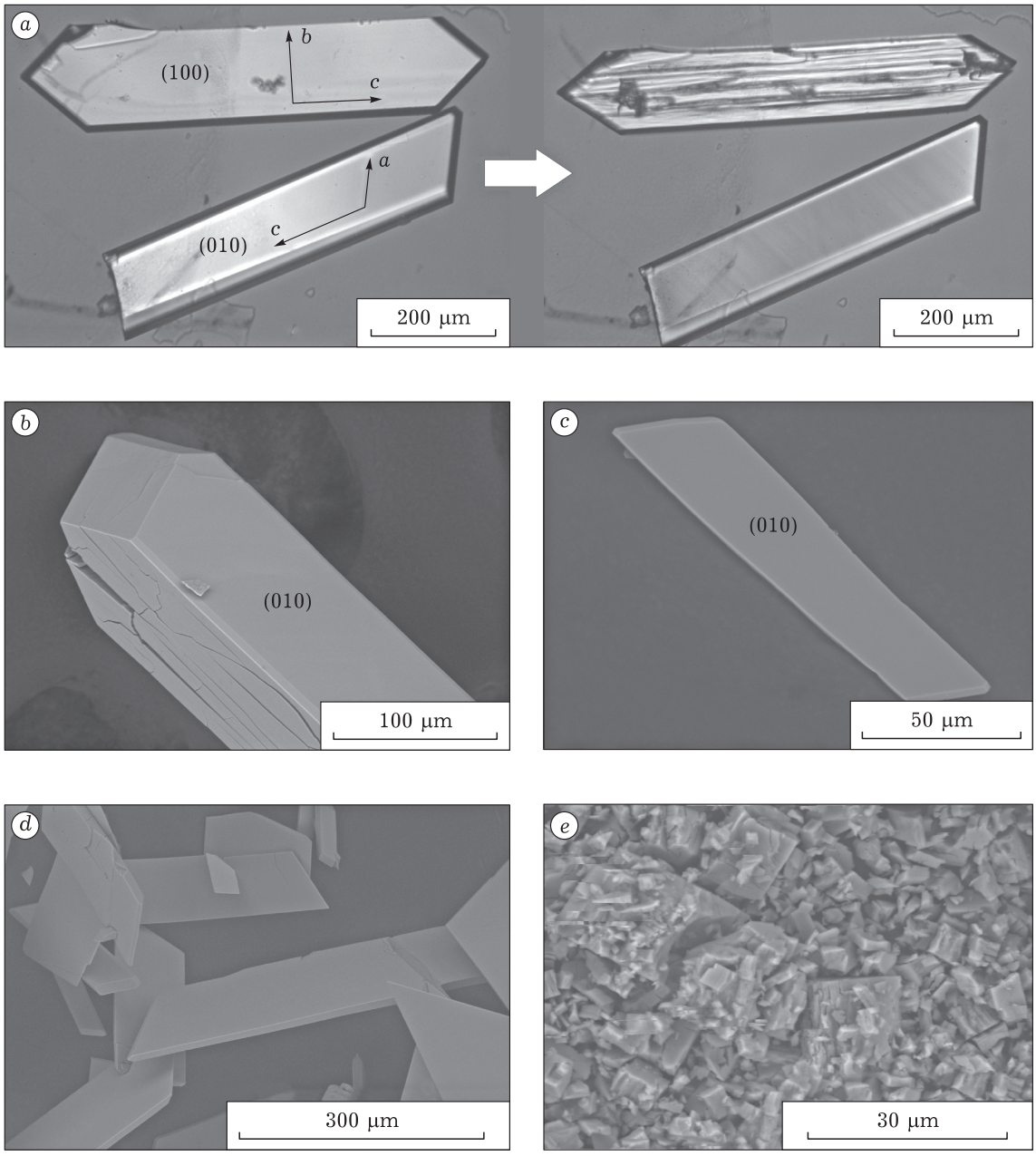

Fig. 2. SEM photographs of initial $Ce_2(C_2O_4)_3 \cdot 10H_2O$ crystals and the products of its dehydration under different conditions: *a* – dehydration in the air, crystals with habit planes (010) and (100); *b* – destruction of thick crystals parallel to the (010) face during dehydration in vacuum; *c* – crystal with thickness <20 μm after dehydration in vacuum; *d* – pseudomorph formation during dehydration in vacuum or in the air; *e* – destruction of precursor crystals during slow dehydration (under increased water vapour pressure).

slow dehydration under quasi-equilibrium conditions (a closed container with a small hole providing slow removal of water from the sample, temperature 120–175 °C, long time of the process up to 120 h) the crystal is destroyed into separate blocks less than 5 μm in size (see Fig. 2, *e*). This is an unexpected result. As a rule, thermal decomposition under the conditions close to equilibrium promotes a decrease in deficiency and an increase in the size of the particles of reaction product (for example, this is the case for thermal decomposition of calcite [25]). The main reason of the influence of dehydration conditions on the morphology of reaction product is connected with the formation of various polymorphous modifications of cerium (III) oxalate hexahydrate. Two different topotaxial structural transformations are observed during the dehydration of $Ce_2(C_2O_4)_3 \cdot 10H_2O$.

Investigation with the optical methods showed that dehydration in vacuum or in the air involves

an anisotropic change of the size of crystals: a substantial decrease in the size along the *b* axis (~30 %) and insignificant deformation along the directions of *a* and *c* (~5 %). Axis *b* is perpendicular to cerium oxalate layers, so the observed crystal deformation is the evidence of a decrease in the distance between the layers with the conservation of layer parameters.

We suppose that dehydration in vacuum or in the air proceeds as follows. At first, partial removal of mobile interlayer water occurs, and a solid solution of water vacancies in the initial structure is formed, which is so-called vacancy structure. Running over the region of the existence of the vacancy structure is accompanied by the appearance of plate-like segregates growing along the (010) plane, and crystal compression along the *b* axis. Complete filling of crystal volume with plate-like segregates corresponds to the loss of four water molecules, to chemical composition $Ce_2(C_2O_4)_3 \cdot 6H_2O$ and to crystal compression by 18–20 %. The structures with $n < 10$ have been unknown for cerium polyhydrate oxalate $Ce_2(C_2O_4)_3 \cdot nH_2O$. However, analysis of the structures of hexa- and tetrahydrates of praseodymium oxalate tetrahydrates [26–28] (the nearest neighbour of cerium in the lanthanide row) showed that the formation of dimers composed of polyhedrons is characteristic of these structures. Cross-linking of the polyhedra is connected with the removal of one water molecule from the nearest surroundings of the metal cation and the insertion of oxygen of the oxalate ion from the neighbouring polyhedron. It may be assumed that the formation of cerium (III) oxalate hexahydrate also involves the removal of water molecules from the nearest surroundings of cerium. The position of the removed water molecule in the coordination polyhedron is occupied by oxygen of the oxalate ion from the nearest coordination polyhedron of the neighbouring layer. As a result, re-linking of the neighbouring cerium oxalate layers occurs, with a substantial decrease in the distance and with the formation of strong bonds fixing the layer structure and providing the conservation of its parameters in further dehydration. It was demonstrated that X-ray amorphous product was formed as a result of water removal. This may be connected with the fact that cross-linking of the layers proceeds in a disordered manner and leads to the loss of the long-range order in the positions of atoms. During further dehydration, water is removed from the interlayer space, and the hydrate $Ce_2(C_2O_4)_3 \cdot nH_2O$ is formed ($n < 3$, where n depends on dehydration conditions). This transformation is accompanied by a further decrease in the distance between cerium – oxalate layers and the compression of the crystal along the *b* axis by 30 %. Complete removal of water from dehydration product is observed only during the decomposition of oxalate ($T > 250$ °C).

Faceting of $Ce_2(C_2O_4)_3 \cdot nH_2O$ crystals is presented in Fig. 1, *b*. Mainly plate-like crystals with two types of faceting grow. The crystals with the first type of faceting have the dominant (100) face, while the basal face in the crystals of the second type is the (010) face. It should be stressed that the crystals with the habit of the first type (100) grow in the medium with low pH and were obtained mainly through recrystallization from saturated solutions, while the crystals of (010) habit are synthesized according to a standard procedure through the joint addition of the diluted solutions of the reagents. Anisotropy of deformation during dehydration is the reason why the thickness and habit of the crystals have a substantial effect on the morphology of dehydration product. The photographs of the crystals of (100) habit (upper crystal) and (010) habit (lower crystal) before and after dehydration are presented in Fig. 2, *a*. One can see that the width of the crystal of (100) habit decreased substantially, and cracks appeared on the surface. Quite contrary, the changes in the size of the crystals of (010) habit are insignificant. The destruction of the crystals occurs mainly along the planes (010) (see Fig. 2, *b*). The scale of destruction exceeds 10 μm, so the crystals of (010) habit with the thickness of less than 20 μm are not destroyed (see Fig. 2, *c*). So, crystal faceting and size affect the dispersion of the product formed through dehydration of the precursor.

Unlike for dehydration in vacuum or in the air, the reaction carried out under quasi-equilibrium conditions leads to the formation of crystal products, and dispersing of initial crystals into the particles less than 5 μm in size occurs (see Fig. 2, *e*). It was established by means of powder diffractometry that in this case the phases $Ce_2(C_2O_4)_3 \cdot 6H_2O$ and $Ce_2(C_2O_4)_3 \cdot 3.5H_2O$ are formed. The destruction of the sample occurs at the stage of hexahydrate formation. Analysis of diffraction patterns showed that the structure of cerium (III) oxalate hexahydrate obtained under quasi-equilibrium conditions is similar to the structure of samarium (III) and europium (III) oxalate hexahydrate [29, 30]. This structure be-

longs to the monoclinic system and has the spatial symmetry group $P2_1/c$, *i.e.* the space symmetry group remains unchanged in the structural transformation. Similarly to initial decahydrate, cerium ions in cerium (III) oxalate hexahydrate coordinate 9 oxygen atoms; the crystal structure is composed of metal-oxalate layers, too, but layer structure undergoes substantial changes (see Fig. 1, *d*). The shape of the cell of metal-oxalate network changes from hexagonal to nearly rectangular (see Fig. 1, *c*, *d*). Interlayer crystal water is completely absent from the structure. It should be stressed that the existence of the monoclinic phase of cerium (III) oxalate hexahydrate has not been reported before, and it was discovered for the first time in this work. In [29] we carried out a detailed investigation of the mechanism of structural transformation during the dehydration of $Sm_2(C_2O_4)_3 \cdot 10H_2O$. We suppose that a similar mechanism takes place also in the formation of monoclinic $Ce_2(C_2O_4)_3 \cdot 6H_2O$. The course of reaction involves the removal of the molecules of outer-shell water and the deformation of the metal-oxalate network. The structure of $Ce_2(C_2O_4)_3 \cdot 6H_2O$ may be obtained from the structure of decahydrate through a shift of each (100) plane along the [00-1] direction by approximately 1/2 *c* and compression in the direction perpendicular to these planes. As a result of structural deformation, the shape of the network cell becomes nearly rectangular.

In situ observation with optical methods showed that the reaction proceeds in a localized manner. Particles start to chip off the crystal at a definite site, the front of destruction is formed, and it moves over the crystal. As a result, the crystal goes into many pieces non-connected with each other. The motion of reaction front over the crystal involves shifts and turns of the crystal and the formed particles. The observed transformation possesses all morphological features prone to displacive or martensite phase transitions. A specific feature of this transformation is its occurrence as a result of the change of the chemical composition, namely the removal of water molecules from the crystal, rather than temperature or pressure change.

So, the morphology of dehydration product is affected by the size, crystal faceting (habit), and reaction conditions (see Fig. 2). One may govern the dispersion of the dehydration product by changing these parameters. As we have already mentioned above, thin plate-like (010) crystals with the thickness of less than 20 μm are not destroyed during dehydration (see Fig. 2, *c*, *d*). Destruction is observed in thick crystals (maybe due to the formation of elastic strain sufficient for the destruction of the sample) and in the crystals with the developed (100) face, in the plane of which the crystal is compressed. Destruction always takes place along the (010) planes. In the case of the reaction carried out under quasi-equilibrium conditions, the crystals are destroyed into the particles of micron size (see Fig. 2, *e*).

Heating in the air leads to the oxidative thermolysis of cerium (III) oxalate hexahydrate. Cerium dioxide is formed as a pseudomorph. The photographs of two $Ce_2(C_2O_4)_3 \cdot 10H_2O$ crystals of different thickness heated in the air (1 °C/min) are shown in Fig. 3, *a*. The thin crystal remains transparent after dehydration. A thicker crystal exhibits destruction, which causes light scattering. The transparency of the thin crystal is conserved after the formation of cerium dioxide. The diffraction pattern of the product of oxidative thermolysis is presented in Fig. 3, *b*. The reaction product is cerium dioxide with fluorite structure. Broad reflections are the evidence of a small size of the particles. Calculation of crystallite size was carried out using the Rietveld method in the Topas 4.2 software (Bruker AXS, Germany). The average size of the crystallites was about 5 nm. According to the data on low-temperature nitrogen adsorption, the specific surface of the resulting CeO_2 is 140–150 m^2/g. If we assume that the shape of cerium dioxide particles is isotropic, particle size corresponding to this value of specific surface is about 6 nm. So, it may be concluded that the crystallite size is close to the size of cerium dioxide particles.

The high-resolution electron microphotograph of the product of oxidative thermolysis and the electron diffraction pattern are shown in Fig. 3, *c*. The resulting cerium dioxide is composed of crystallites 5–6 nm in size. The ring diffraction maxima at the electron diffraction pattern are the evidence of crystallite disorientation in the sample. This may be connected with the fact that the structures of the dehydrated sample and the final product are strongly different from each other, no orientation correspondence is observed between them.

Measurements of crystal size before and after reaction allow determining the volume shrinkage during the reaction and the porosity of the pseudomorph. For the formation of the pseudomorph of cerium dioxide, porosity is about 40 %. This value is in good agreement with the value of pore

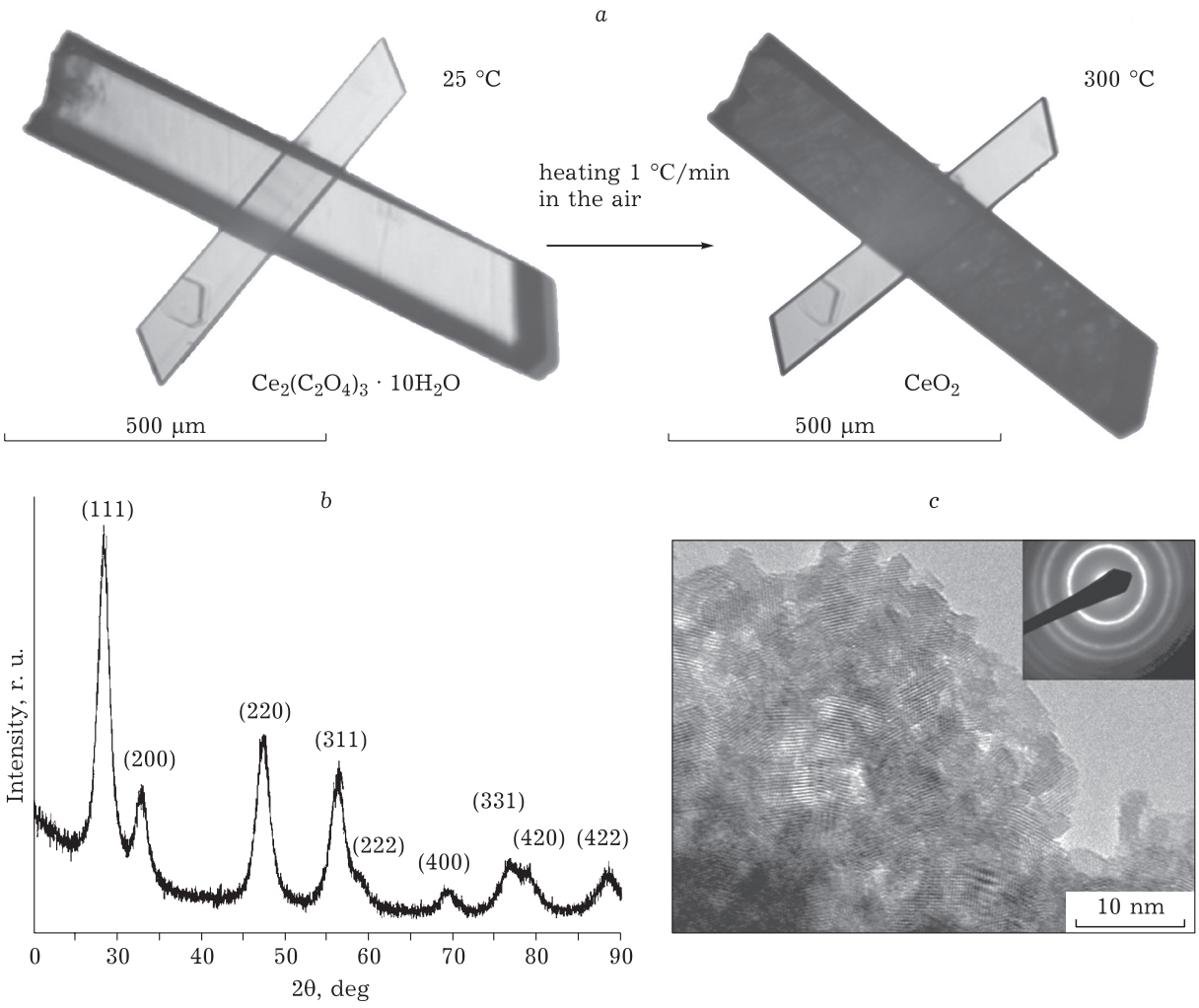

Fig. 3. Morphological changes during thermal decomposition of precursor crystals in the air: a thicker crystal is destroyed and scatters light, while the thinner crystal remains transparent till the end of transformation (*a*); powder diffraction pattern of the obtained CeO_2 (*b*); microphotograph and electron diffraction pattern of the obtained CeO_2 (TEM) (*c*).

volume, which is 0.092 cm^3/g, as determined from adsorption measurements.

The effect of annealing temperature on the process of enlargement of cerium dioxide particles in the pseudomorph was studied. Long-term annealing of the resulting cerium dioxide at 250 °C did not have any noticeable effect on its texture characteristics. However, at a temperature above 500 °C substantial enlargement of cerium dioxide particles started. After sample exposure for 1 h at 500 °C, the specific surface was 37 m^2/g, and at 750 °C it decreased to 2 m^2/g.

The general scheme of morphological changes during the thermal decomposition of cerium (III) oxalate decahydrate is presented in Fig. 4. The final product of the reaction is composed of the compact aggregates of CeO_2 nanoparticles connected by necks and separated by pores. It was demonstrated that the qualitative change of the morphology under thermal decomposition of $Ce_2(C_2O_4)_3 \cdot 10H_2O$ takes place at the first and the last stages of the reaction, which are characterized by the largest shrinkage values and substantial structural rearrangements. During the formation of $Ce_2(C_2O_4)_3 \cdot 6H_2O$ in vacuum or in the air, uniform compression of thin crystals without destruction occurs, or the destruction of thick crystals into coarse blocks (more than 10 μm). During slow dehydration at a temperature of 120 °C and higher, destruction into blocks less than 5 μm in size occurs. So, the size and shape of the particles may be governed at the stage of the formation of $Ce_2(C_2O_4)_3 \cdot 6H_2O$. The size of the particles forming the 3*D*-structure of the aggregates and the internal porosity are determined by the final stage of the reaction, which is the formation of cerium dioxide. In this work, we succeeded in obtaining a pseudomorph composed of

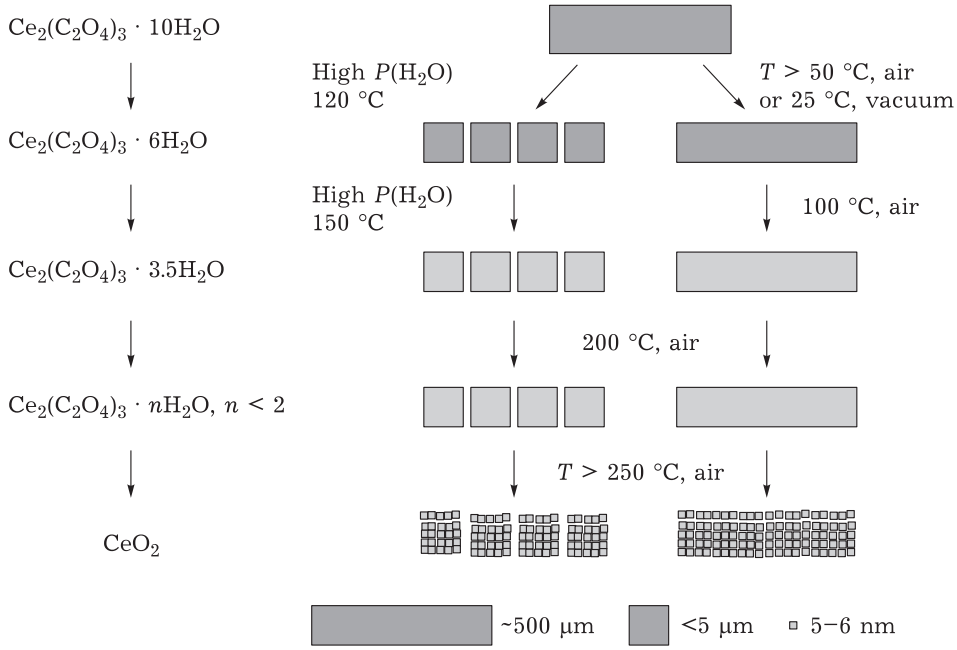

Fig. 4. General scheme of the control of the morphology of final product (CeO_2) during thermal decomposition of $Ce_2(C_2O_4)_3 \cdot 10H_2O$.

cerium oxide particles 5–6 nm in size, with specific surface 140–150 m^2/g and porosity 40 %. These values are a record for cerium dioxide obtained by means of thermal decomposition from various precursors. Controllable annealing allows one to carry out the enlargement of the microstructure to the necessary size of the particles comprising the pseudomorph. So, the aggregates of cerium dioxide particles with the required size, dispersion and porosity may be obtained by regulating initial dimensions and shape of precursor crystals, conditions of the reaction and subsequent thermal treatment.

CONCLUSION

The major factors affecting the morphology of CeO_2, the final product of thermal decomposition of $Ce_2(C_2O_4)_3 \cdot 10H_2O$, were revealed.

Reaction conditions under which CeO_2 is formed as pseudomorphs with the conservation of the size and shape of precursor crystals were determined. This allows performing the morphological design of the material as early as at the stage of precursor synthesis: the size and shape of precursor crystals will determine the morphology of CeO_2.

It is shown that the conditions of $Ce_2(C_2O_4)_3 \cdot 10H_2O$ dehydration have a substantial effect on the morphology and crystal structure of the product: the shape of initial crystals is retained after dehydration in vacuum or in the air, in other words, a pseudomorph is formed; if dehydration is carried out at increased water pressure, the formation of the crystal phase occurs along with crystal dispersion into particles less than 5 μm in size. Two versions of structural transformations during the dehydration of $Ce_2(C_2O_4)_3 \cdot 10H_2O$ crystals are proposed. They are implemented under different reaction conditions. These transformations cause different transformations of the initial structure, which leads to differences in the scale of destruction, sizes and shapes of crystals.

It is demonstrated that an essential factor to control the morphology during precursor dehydration in vacuum or in the air is the thickness of initial crystals. Thin lamellar (010) crystals with the thickness less than 20 μm are not destroyed, unlike for thick crystals and the crystals with the developed (100) face, in the plane of which the crystal compression occurs. It is necessary to stress that the crystals that are not subjected to destruction remain transparent fore visible light until the transformation is completed (until the CeO_2 is obtained).

The final product of the reaction, CeO_2, is formed as a pseudomorph composed of the particles 5–6 nm in size. Nanoparticles in the pseudomorph are bound through contacts and form a porous three-dimensional framework, a 3*D*-structure. Pores occupy about 40 % of the pseudo-

morph volume. The investigation by means of TEM showed that the crystallites in the pseudomorph have an arbitrary orientation. Long-term annealing of the resulting cerium dioxide at 250 °C has no substantial effect on its texture characteristics. However, at a temperature higher than 500 °C substantial enlargement of cerium dioxide particles starts.

Acknowledgements

The work was carried out within the State Assignment for the ISSCM SB RAS (AAAA-A17-117030310281-3).

REFERENCES

1 USA Pat. No. 4738947A, 1988.
2 Tong Y., Rosynek M. P., Lunsford J. H., *J. Phys. Chem.*, 1989, Vol. 93, No. 8, P. 2896–2898.
3 Ganduglia-Pirovano M. V., *Catal. Today*, 2015, Vol. 253, P. 20–32.
4 Zha S., Xia C., Meng G., *J. Power Sources*, 2003, Vol. 115, No. 1, P. 44–48.
5 Popov M. P., Maslennikov D. V., Gainutdinov I. I., Gulyaev I. P., Zagoruiko A. N., Nemudry A. P., *Catal. Today*, 2019, Vol. 329, P. 167–170.
6 Janos P., Ederer J., Pilarova V., Henych J., Tolasz J., Milde D., Opletal T., *Wear*, 2016, Vol. 362–363, P. 114–120.
7 Jasinski P., Suzuki T., Anderson H. U., *Sens. Actuators. B*, 2003, Vol. 95, No. 1–3, P. 73–77.
8 Caputo F., De Nicola M., Sienkiewicz A., Giovanetti A., Bejarano I., Licoccia S., Traversab E., Ghibelli L., *Nanoscale*, 2015, Vol. 7, No. 38, P. 15643–15656.
9 Zholobak N. M., Ivanov V. K., Shcherbakov A. B., Shaporev A. S., Polezhaeva O. S., Baranchikov A. Ye., Spivak N. Ya., Tretyakov Yu. D., *J. Photochem. Photobiol., B*, 2011, Vol. 102, No. 1, P. 32–38.
10 Ivanov V. K., Shcherbakov A. B., Usatenko A. V., *Russ. Chem. Rev.*, 2009, Vol. 78, No. 9, P. 855–871.
11 Xu C., Qu X., *NPG Asia Mater.*, 2014, Vol. 6, No. 3, P. e90.
12 Guan Y., Li M., Dong K., Gao N., Ren J., Zheng Y., Qu X., *Biomaterials*, 2016, Vol. 98, P. 92–102.
13 Rocca A., Moscato S., Ronca F., Nitti S., Mattoli V., Giorgi M., Ciofani G., *Nanomedicine*, 2015, Vol. 11, No. 7, P. 1725–1734.
14 Ivanov V. K., Polezhaeva O. S., Kopitsa G. P., Fedorov P. P., Pranzas K., Runov V. V., *Russ. J. Inorg. Chem.*, 2009, Vol. 54, No. 11, P. 1689–1696.
15 Ivanov V. K., Polezhaeva O. S., *Russ. J. Inorg. Chem.*, 2009, Vol. 54, No. 10, P. 1528–1530.
16 Sanchez-Dominguez M., Liotta L. F., Di Carlo G., Pantaleo G., Venezia A. M., Solans C., Boutonnet M., *Catal. Today*, 2010, Vol. 158, No. 1–2, P. 35–43.
17 Kockrick E., Schrage C., Grigas A., Geiger D., Kaskel S., *J. Solid State Chem.*, 2008, Vol. 181, No. 7, P. 1614–1620.
18 Yu C., Zhang L., Shi J., Zhao J., Gao J., Yan D., *Adv. Funct. Mater.*, 2008, Vol. 18, No. 10, P. 1544–1554.
19 Cherepanova S. V., Ancharova U. V., Bulavchenko O. A., Venediktova O. S., Gerasimov E. Yu., Leontyeva N. N., Matvienko A. A., Maslennikov D. V., Pakharukova V. P., Sidelnikov A. A., Tsybulya S. B., Chuzhik S. A., Yatsenko D. A. Nanostructured Oxides [in Russian], Novosibirsk, Novosibirsk State University, IPTs NGU, 2016. 206 p.
20 Sidelnikov A. A., Chizhik S. A., Matvienko A. A., Sharafutdinov M. R., *Chem. Sustain. Devel.* [in Russian], 2014, Vol. 22, No. 4, P. 347–358.
21 Maslennikov D. V., Matvienko A. A., Sidelnikov A. A., Chizhik S. A., *Mater. Today: Proc.*, 2017, Vol. 4, P. 11495–11499.
22 Maslennikov D. V., Matvienko A. A., Chizhik S. A., Sidelnikov A. A., *Ceram. Int.*, 2019, Vol. 45, No. 3, P. 4137–4141.
23 Hansson E., *Acta Chem. Scand.*, 1970, Vol. 24, P. 2969–2982.
24 Wang P., Fan R. Q., Liu X. R., Wang L. Y., Yang Y. L., Cao W. W., Yang B., Hasi W., Su Q., Mu Y., *Cryst. Eng. Comm.*, 2013, Vol. 15, No. 10, P. 1931–1949.
25 Beruto D., Barco L., Searcy A. W., *J. Am. Ceram. Soc.*, 1984, Vol. 67, No. 7, P. 512–516.
26 Trombe J. C., Jaud J., *J. Chem. Crystallogr.*, 2002, P. 19–26.
27 Hao C.-J., Xie H., *Acta Crystallogr. Sect. E: Struct. Rep. Online*, 2012, Vol. 68, No. 4, P. m444.
28 Athar M., Qureshi A. M., Li G., Shi Z., Feng S., *Indian J. Chem.*, 2012, P. 7.
29 Matvienko A. A., Maslennikov D. V., Zakharov B. A., Sidelnikov A. A., Chizhik S. A., Boldyreva E. V., *IUCrJ*, 2017, Vol. 4, P. 588–597.
30 Trollet D., Romero S., Mosset A., Trombe J. C., *C. R. Acad. Sci., Ser. IIb: Mec., Phys., Chim., Astron.*, 1997, Vol. 325, No. 11, P. 663–670.